

A novel approach to monitor hemodynamics of carotid artery

Wei-Jie Yang¹ and *Po-Ling Kuo^{1,2}

¹Graduate Institute of Biomedical Electronics and Bioinformatics, ²Department of Electrical Engineering, National Taiwan University, Taipei, Taiwan

*Corresponding author's email: poling@cc.ee.ntu.edu.tw

ABSTRACT

The hemodynamic of carotid artery is an important indicator for monitoring brain circulation during various clinical procedures and conditions such as cerebral vascular accident, brain surgery, progress of traumatic brain injury, and cardiac catheterization. Ultrasonic based methods, such as Doppler measurement, M and B mode imaging, are the most common approaches to non-invasively monitor the hemodynamic of carotid arteries. However these methods require expensive equipment and proficient clinicians who are impossible to continuously monitor the hemodynamic throughout the procedures. In this work, we proposed a novel approach to monitor the flow rate of carotid artery using the pulsatile pressure measured on neck. A theoretical framework quantitatively determining the transfer function between the neck surface pressure and the carotid flow rate was derived based on Navier-Stokes equation and solutions of a Lamé problem. The carotid flow simulation was conducted with a phantom system consisting of a carotid phantom made of biomimetic material, a blood flow simulator, an ultrasonic imaging system, and a MEMS-based fiber optic pressure sensor. The experimental data fit well to the theoretic predictions. The waveforms between the measured and predicted flow velocity show high similarity except mild distortion due to errors of parameters approximation. Our results promise the clinical potential of the proposed approach.

1. INTRODUCTION

Cerebrovascular accidents (CVA), or stroke, is a major cause of death worldwide. More than 60% of the patients die in 5 years after stroke, and half of survivors require long-term medical care due to disability (Hankey 2003). Although the death rate of CVA has reduced in recent years because of the improvements in medical condition, the incidence rate of CVA shows no sign of decrease and eventually will raise the total population of CVA patients. The long-term medical care to patients will definitely become the burden of their families and even the social economy. Thus, the issue about how to prevent CVA from occurring and reduce the severity of patients is of great urgency.

Clinically, cerebral blood flow (CBF) is an important indicator for the prevention and treatment guide of cerebral vascular accident. For example, when the carotid artery which provides blood to the cerebral narrows, the cerebral blood flow reduces and a higher incidence rate of stroke is observed (AbuRahma 2002). After surgeries like carotid artery stenting or carotid endarterectomy, it is easier to give rise to thrombus

formation and requires continuous monitoring of CBF to prevent the occurrence of stroke on account of artery narrowing (Riles 1994). Therefore, long-term monitoring of carotid artery hemodynamic and a real time warning system will possibly become the effective method to reduce incidence rate of CVA.

At present, clinical methods to estimate cerebral blood flow can be classified as invasive and non-invasive methods. Invasive monitoring uses catheters or cuffs with sensors on them to measure the blood flow by mechanisms such as electromagnetic induction (Mason 1970) and Doppler effects (Doucette 1992). Although these methods have high accuracy, the associated risk, the expense of equipment, and the medical conditions prevent it from long-term monitoring. Noninvasive measurements include laser Doppler flowmeter (Ohashi 2009), pulsed ultrasonic Doppler flowmetry (Tortoli 2002) and magnetic resonance phase velocity mapping (Shimizu 1986). These methods are at low risk and with fewer limitations to the medical condition while the cost of instrument and need of well trained operator make them unsuitable for long-term measurement at home or general ward.

In addition to directly measure the flow velocity, we can estimate this quantity from the artery pressure waveform. Two major noninvasive methods for measuring artery pressure are volume-clamped photoplethysmography (Penaz 1992) and applanation tonometry (Drzewiecki 1983). Photoplethysmography uses the inflatable cuff mounted with infrared transmission plethysmograph to measure the volumetric change of finger artery. The optical mechanism restricts it to only measure the arteries near the skin surface which is not the case of carotid artery. Applanation tonometry applies pressure on the arterial noninvasively to make it flatten and uses the tonometer to measure the pressure. Theoretically the measured pressure value will be equivalent to the arterial blood pressure. The limitations of this method for our objective are its difficulty to fix the device on neck and risks of pressuring the carotid artery in a long period of time.

Given the disadvantages of the above methods, we hope to find one low-cost, non-invasive mean that is suitable to long term monitoring of the carotid artery flow. One possible method is to directly measure the pressure on the neck surface without applanation. The connection between artery blood flow and surface pressure can be described by the following figure.



Fig. 1 Relation diagram between blood flow and surface pressure

Given some assumptions about the geometry of the neck, carotid artery and property of fluid, we can relate the blood flow to surface pressure from Navier-Stokes equation and transfer function derived in (Timoshenko 1970).

The rest of our paper is organized as follows: Basic theories mentioned in the relation diagram are introduced in Section II. Our experimental setup is explained in Section III. Section IV gives our result on phantom study and includes the discussion. Finally we close the paper with conclusion and future work in Section V.

2. THEORY

2.1 Mechanical model for carotid artery

The mechanical model for carotid artery and its surrounding tissues can be approximated by two parallel cylinders which are full of fluid and buried in a larger cylindrical. Because of axial symmetry and the assumption of the model as plane strain, we can further simplify it to half of the transverse plane (Fig. 2(b)).

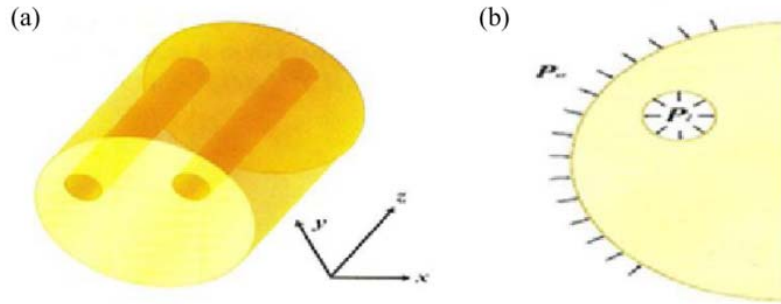


Fig. 2 (a) Three dimensional mechanical model for carotid artery. (b) Transverse plane view of the model shown in (a)

From the analytical solution of the Lamè problem, the surface pressure P_s of the cylindrical is solved (Timoshenko 1970). In Lamè problem, we assume that the inner cylindrical is under pressure P_i and the outer cylindrical is under pressure P_o as shown in Fig.2(b) and define R_i and R_o to be the radius of the inner cylindrical and the distance from the center of inner cylindrical to the surface. If the material is nearly incompressible (Poisson ratio $\nu \sim 0.45$), homogeneous and purely elastic (with elasticity E), the stress along radial and tangential direction σ_{rr} , $\sigma_{\theta\theta}$ on the transverse plane and the displacement along radial direction u_{rr} can be expressed as

$$\sigma_{rr}(r) = -P_o - \frac{\frac{R_o^2}{r} - 1}{\frac{R_o^2}{R_i} - 1} (P_i - P_o) \quad (1)$$

$$\sigma_{\theta\theta}(r) = -P_o + \frac{\frac{R_o^2}{r} + 1}{\frac{R_o^2}{R_i} - 1} (P_i - P_o) \quad (2)$$

$$u_{rr}(r) = \frac{1+\nu}{E(\frac{R_o^2}{R_i} - 1)} \left\{ \frac{R_o^2}{r} (P_i - P_o) + (1 - 2\nu)(P_i - \frac{R_o^2}{R_i} P_o) r \right\} \quad (3)$$

Illustration of σ_{rr} , $\sigma_{\theta\theta}$ and u_{rr} is shown in Fig. 3. It is assumed that stress along radial direction provided by the pressure sensor and $\sigma_{\theta\theta}$ are balanced to restrict the displacement at the surface to be 0 ($u_{rr}(R_o) \approx 0$). Substituting this condition into Eq. (3) gives the pressure transfer function between surface pressure ($P_s \approx P_o(R_o)$) and inner pressure P_i

$$P_S \approx \frac{2(1-\nu)}{1+(1-2\nu)\frac{R_o^2}{R_i^2}} P_i \quad (4)$$

To verify the equation's accuracy, we estimate the displacement relation between arterial wall and the phantom surface and compare it with Eq. (3).

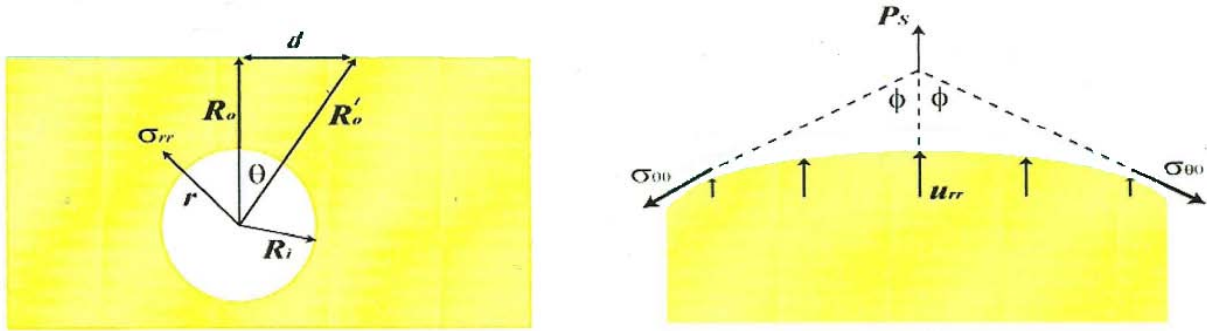


Fig. 3 Geometric relation for the Lamé problem

2.2 Blood flow estimation

Given the assumptions that blood is a incompressible and constant viscosity fluid, the axial velocity along the artery with radial symmetry is much larger than other directions and blood has no rotational motions, The blood velocity can be characterized by the simplified Navier-Stokes equation (Nichols 2011)

$$\rho \frac{\partial v}{\partial t} = \eta \left(\frac{\partial^2 v}{\partial r^2} + \frac{1}{r} \frac{\partial v}{\partial r} \right) + \frac{\partial P}{\partial z} \quad (5)$$

where v is blood flow velocity along the axis of artery (z direction), ρ · η are blood's density and kinematic viscosity, P is blood pressure, r is the position parameter along artery radial direction and t is time parameter. If we expand the gradient of pressure at position z_0 by Fourier series as

$$\frac{\partial P}{\partial z} \Big|_{z_0} = \frac{1}{2} \sum_{n=-\infty}^{\infty} \Phi(n) e^{in\omega t} \quad (6)$$

By substituting one harmonic component of $\frac{\partial P}{\partial z}$ ($\Phi(t) = A^* e^{i\omega t}$, A^* is a complex number) into Eq. (5) and integrating the velocity along r direction, the solution of blood flow Q is obtained

$$Q = \frac{\pi R^2 A^*}{i\omega\rho} \left(1 - \frac{2J_1(\alpha i^{\frac{3}{2}})}{\alpha i^{\frac{3}{2}} J_0(\alpha i^{\frac{3}{2}})} \right) e^{i\omega t}, \alpha = \sqrt{\frac{R^2 \omega}{\eta}} \quad (7)$$

where J_0, J_1 is the zeroth and first order Bessel function, R means radius of artery. And the corresponding blood flow for real part of $\Phi(t)$ ($P_0 \cos(\omega t - \phi)$) is written as (Nichols 2011)

$$Q = \frac{\pi R^2 P_0}{\omega \rho} \left(1 - \frac{2J_1(\alpha i^{\frac{3}{2}})}{\alpha i^{\frac{3}{2}} J_0(\alpha i^{\frac{3}{2}})} \right) \sin(\omega t - \phi) \quad (8)$$

Due to practical limitations, we can't get the exact spatial gradient of pressure ($\frac{\partial P}{\partial z}$). Thus the time gradient of pressure ($\frac{\partial P}{\partial t}$) is used to approximate it by the following relation

$$\frac{\partial P}{\partial t} = \frac{\partial P}{\partial z} \frac{\partial z}{\partial t} = V_p \frac{\partial P}{\partial z} \quad (9)$$

where V_p is pulse wave velocity (PWV). Assume one harmonic component of the measured pressure signal is $\Psi_{z_0}(t) (= P_0 \cos(\omega t - \phi_1))$, we can use $\Psi_{z_0}(t)$ and Eq. (9) to derive another form of Eq. (8)

$$Q = \frac{\pi R^2 P_0}{\rho} \frac{1}{V_p} \left(1 - \frac{2J_1(\alpha i^{\frac{3}{2}})}{\alpha i^{\frac{3}{2}} J_0(\alpha i^{\frac{3}{2}})} \right) \sin(\omega t - \phi_1 + \frac{\pi}{2}) \quad (10)$$

Because of the low frequency characteristic of pressure wave in experiments, only harmonic components from 0 to 20 Hz is added up to form the estimated flow. The quantity divided by πR^2 , which is average flow velocity, is then compared with the signal estimated by Doppler ultrasound.

Pulse wave velocity (PWV) is commonly measured by the foot-to-foot technique (Benthin 1991). This technique obtains the PWV value by measuring the transit time delay of "foot" point of the wave over a certain distance. The wall displacements at different measurement sites are used here to compute PWV. The methods to choose foot point include maximum amplitude and intersecting tangent point. Intersecting tangent point is at the intersection of a tangent line to the initial upstroke of the waveform and a horizontal line through the minimum point (Chiu 1991).

3. EXPERIMENTAL ARCHITECTURE

In order to verify the pressure-flow velocity connection and displacement transfer function, we built a system like the following figure (Fig.4). The phantom used here was made of plastic and had a hollow cylinder with radius of 2.5 mm inside it. The cylinder

was filled with blood mimicking fluid(BMF-US, Shelly Medical Imaging Tech., Toronto, Ontario, Canada). The purpose of the phantom was to model the simplified mechanical model for carotid artery and surrounding tissue. Flow to be monitored was generated by the syringe manually or by the peristaltic pump.

For estimating flow velocity and displacement, Verasonics Research System (Verasonics Inc., Redmond, WA) was utilized. The ultrasound probe, a 5-MHz array ultrasound transducer (L7-4) made of 128 elements with a 0.3mm pitch, was placed on the phantom surface to provide pressure which limited the surface displacement. PRFs for the two measurement were 5kHz and 1kHz. In flow velocity estimation, we transmitted the ultrasound beam with steering angle of 12 degree and only acquired the signal of one element of the array ultrasound transducer. Data was then beamformed and demodulated by Verasonics system and the system could provide us with the in-phase and quadrature signals (IQ signals) to do post-processing. For the sake of synchronizing flow velocity and pressure signals measured by a MEMS-based fiber optic pressure sensor(OPP-M, Opsens inc., Quebec, Canada), trigger signal was sent from Verasonics system to notebook via RS-232 communication when the first ultrasonic wave was transmitted. Upon receiving the trigger signal, program written by Labview sent acquisition instruction to another communication port which was connected with pressure sensor to start sampling the pressure signal.

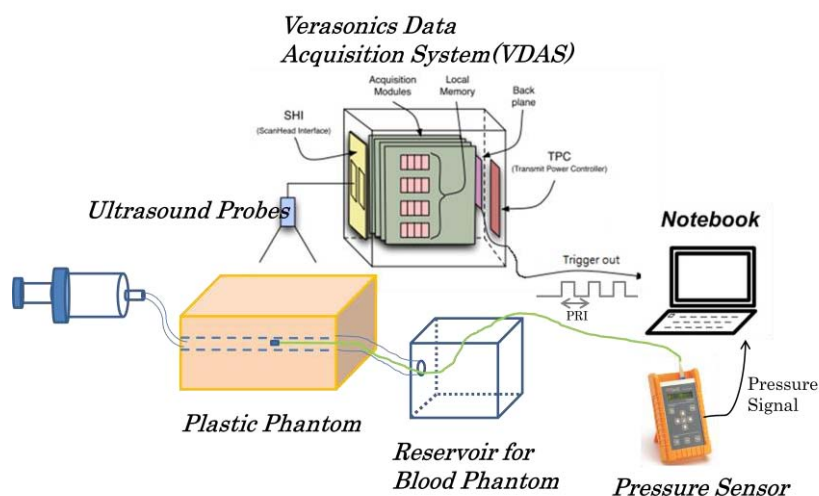


Fig. 4 System for verifying mechanical model and Navier-Stokes equation

4. RESULTS AND DISCUSSIONS

4.1 Displacement transfer function

By 1D autocorrelation method, we monitored the phantom motion under pulsatile flow generated by peristaltic pump. Normalized axial displacement fields at different time instant were illustrated in Fig. 5. The figure captured the motion under a right-to-left flow. Because the lower scatter intensity of the fluid, we could extract only the phantom motion by choosing a proper energy threshold for IQ data. After thresholding, signals

inside the vessel became zeros as shown in the middle part of Fig. 5.

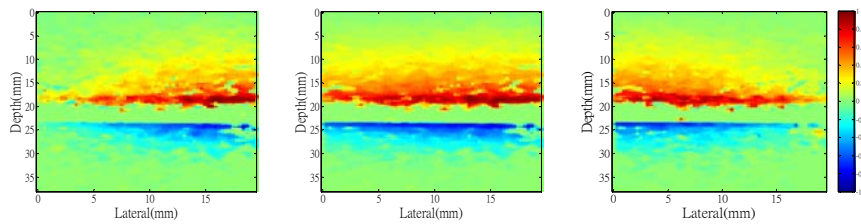


Fig. 5 Normalized axial displacement fields at different time instant

The change of signal's amplitude along depth, or called displacement transfer function, was shown in Fig. 6. The depth with maximum amplitude was selected to be the position of vessel wall and this amplitude was used to normalize the signals along depth. Experimental results appeared good agreement with theory. The plot only showed transfer function at one lateral point and one time instant. This theoretic curve actually fitted well to most experimental results. But when the signal's amplitude was too small, it was possible that the theoretic curve failed to fit and the result transfer function showed little correlation to distance. We could observe this from Fig. 7 which gave the coefficient of determination for each time instant's transfer function.

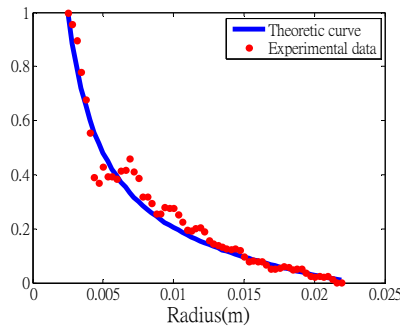


Fig. 6 Displacement transfer function

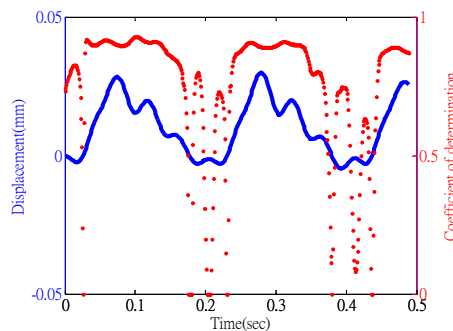


Fig. 7 Displacement signal and its corresponding transfer function's coefficient of determination

The difference between the experimental data and ideal transfer function may

come from the geometry mismatch and existence of viscosity. Geometry of our phantom was different with the Lamé problem. This would inevitably cause some changes in the transfer function. The time dependent characteristic of viscoelastic material also made Eq. (3) insufficient to fully describe this behavior. Another possibility of the difference was due to the assumption of the applied surface pressure. Though the ultrasound transducer provided pressure to limit the surface displacement to be zero, the pressure applied may be larger than expected and cause the difference. Also small vibration from the peristaltic pump may affect the displacement signal.

4.2 Pulse wave velocity estimation

From above results, pulse wave velocity could be calculated by measuring the transit time delay between two measurement point at different lateral location. The mentioned two foot point methods were used to determine the delay. Because array transducer was used in the experiment, 64 velocity profiles were obtained rather than just 2 signals. A better way to utilize this was to determine the regression of time shift and distance. Fig. 8 **Error! Reference source not found.** showed the displacement result with the foot point marked.

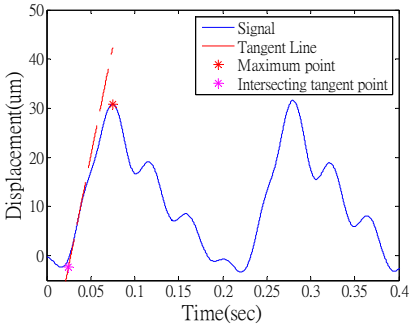


Fig. 8 Displacement signal at one position near wall. Marked points represented the foot points for intersecting tangent point and maximum point.

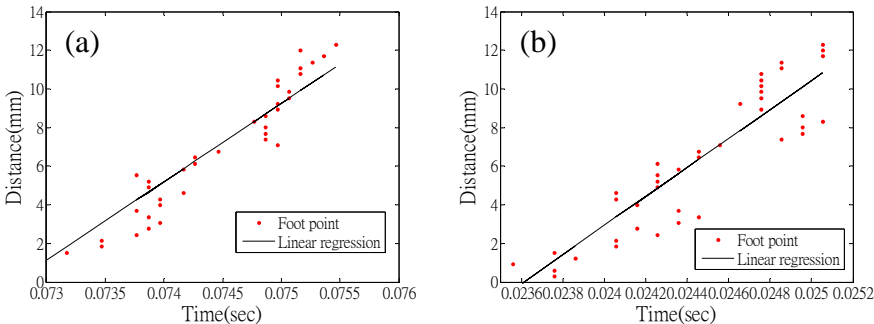


Fig. 9 Time of foot-points at different lateral position.

(a) Maximum point (b) Intersect tangent point.

By linear regression to transit time and distance data, pulse wave velocity was estimated to be the gradient of regression line. The estimated values for the two

methods were 3.41 ± 0.36 m/s and 5.67 ± 0.75 m/s respectively. A larger value of PWV using intersect tangent method was observed. This may result from the lower accuracy of extraction for foot points. As shown in Fig.9, time for several lateral points' foot point appeared to be the same. And a comparatively larger variation to the regression line also showed the problem of this method in our experiment. Coefficient of determination for maximum point was almost 0.9 while the intersect tangent method gave only around 0.7. So we used the PWV estimated by maximum point in the next section.

4.3 Validation of Navier-Stokes equation

Given the PWV value estimated above, we could calculate the flow velocity from pressure signal. Fig. 10 illustrated the flow velocity and pressure signal of one flow pulse which was generated by syringe manually. One of the flow velocity was computed by ultrasound signals using Short-time Fourier transform. The other signal was estimated by Eq. (10) from pressure signal.

The amplitude of the first velocity signals had value of 1 m/s while the reconstructed one was around 0.7 m/s. Though the time for upstroke of the pulse were close for both signals, it was clear that the waveform showed little similarity to the ultrasound one. This situation may result from the approximation of the theory and parameters. For example, we approximated PWV as constant value over a certain frequency range.

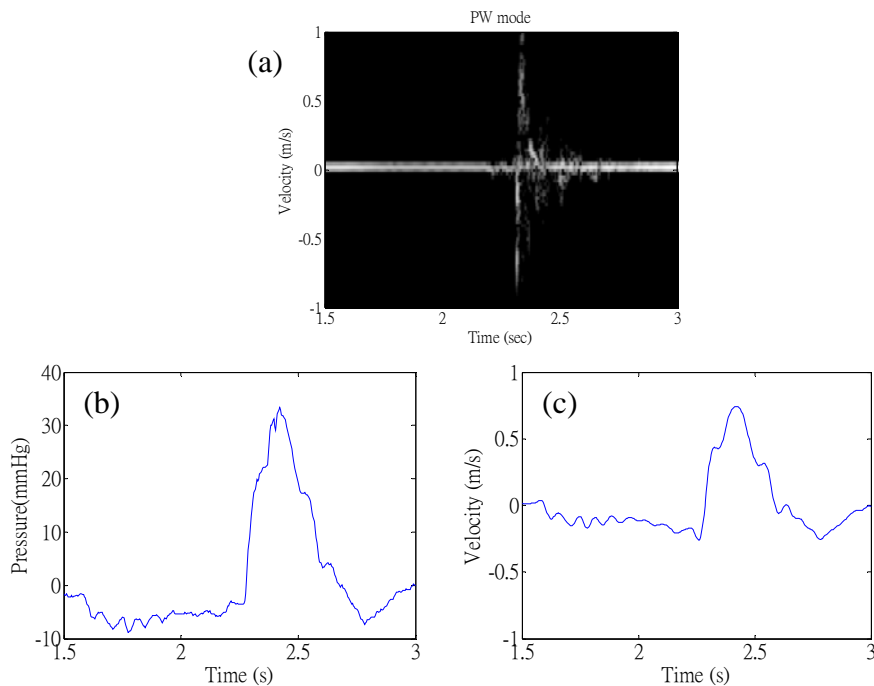


Fig. 10 (a) Flow velocity estimated by ultrasound (b) Pressure signal (c) Flow velocity computed from pressure signal.

Fig.11 gave another experimental result from peristaltic pump. The velocity signal estimated by ultrasound had an average amplitude of 0.25 m/s while the latter had amplitude of 0.14 m/s. Because only the pressure signal at one location was recorded,

we didn't have the DC component of flow velocity. Therefore the reconstructed signal would oscillate around zero.

There were several factors that could cause the difference between the two signals. One of them was the PWV value. Note that the PWV value could affect the estimated flow velocity's amplitude directly. Larger PWV could result in a smaller flow velocity. Also because changing of vessel radius violated the assumption of Navier-Stokes equation, it would have impact on the reconstructed flow velocity.

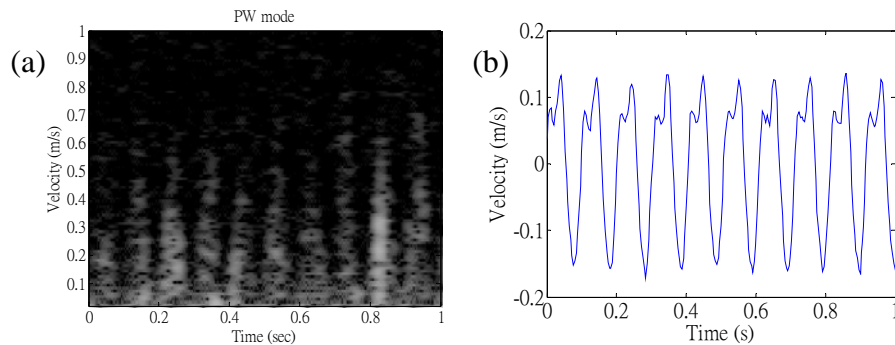


Fig. 11 (a)Flow velocity estimated by ultrasound (b) Flow velocity computed from pressure signal.

5. CONCLUSION AND FUTURE WORK

In this study, a simple mechanical model has been established and the theoretical predictions have been verified by the experimental results. Experimental data fit well to the theoretic model of transfer function while flow velocity computed from pressure signal has close value to one estimated by ultrasound. These validation results show the potential to let us monitor the carotid flow by this approach.

After validation of these theories, a single or array type of pressure sensor is expected to be used to measure the surface pressure continuously and the measurement point should be co-located for flow velocity estimation and the pressure sensor inside the vessel. The surface pressure signal is then converted to flow velocity to do comparison with the one ultrasound estimates.

In our study, we have used a homogeneous phantom to study the hemodynamics of carotid artery. In physiological conditions, the surrounding tissue is inhomogeneous and possibly more viscous. The numerical model utilized here should be corrected for the existence of inhomogeneity and viscosity. Phantom composed of several materials to simulate muscles or connective tissues needs to be built. Future works are focusing on improvement of the model and associated methodologies.

ACKNOWLEDGEMENTS

The authors are grateful for the financial support under grant number NSC101-2220-E-002-011 provided by the National Science Council of Taiwan and grant number 101-EC-17-A-19-S1-174 by provided by the Ministry of Economic Affairs of Taiwan.

REFERENCES

- AbuRahma, A.F., Thiele, S.P. and Wulu, J.T. (2002), "Prospective controlled study of the natural history of asymptomatic 60% to 69% carotid stenosis according to ultrasonic plaque morphology." *J Vasc Surg*, vol. 36, 437-443
- Benthin, M., et al. (1991), "Calculation of Pulse-Wave Velocity Using Cross-Correlation - Effects of Reflexes in the Arterial Tree." *Ultrasound in Medicine and Biology*, 461-469.
- Chiu, Y. C., Arand, P. W., Shroff, S. G., Feldman, T. and Carroll, J. D. (1991), "Determination of pulse wave velocities with computerized algorithms." *American heart journal*, vol. 121, 1460-1470.
- Doucette, J., Corl, P.D., Payne, H., Flynn, A., Goto, M., Nassi, M. and Segal, J. (1992), "Validation of a Doppler guide wire for intravascular measurement of coronary artery flow velocity." *Circulation*, vol. 85, 1899-1911.
- Drzewiecki, G. M., Melbin, J. and Noordergraaf, A. (1983), "Arterial tonometry: review and analysis." *J Biomech*, vol. 16, 141-152.
- Hankey, G.J. (2003), "Long-term outcome after ischaemic stroke/transient ischaemic attack." *Cerebrovascular Diseases*, vol. 16, 14-19.
- Mason, D.T., Gabe, I.T., Mills, C.J., Gault, J.H., Ross, J., Braunwald, E. and Shillingford, J. P. (1970), "Applications of the catheter-tip electromagnetic velocity probe in the study of the central circulation in man." *The American journal of medicine*, vol. 49, 465-471.
- Nichols, W., O'Rourke, M.F. and Vlachopoulos, C. (2011), *McDonald's Blood Flow in Arteries: Theoretical, Experimental and Clinical Principles*, Hodder Arnold.
- Ohashi, A., Kuroyanagi, Y., Kitamura, N., Kinoshita, Y., Kaneko, K. and Yabuta, K. (2009), "Cerebral blood flow monitoring using a novel laser Doppler flowmeter in asphyxiated infants." *Pediatrics International*, vol. 51, 715-719.
- Penaz, J. (1992), "Criteria for set point estimation in the volume clamp method of blood pressure measurement." *Physiological research/Academia Scientiarum Bohemoslovaca*, vol. 41, 5.
- Riles, T.S., Imparato, A.M., Jacobowitz, G.R., Lamparello, P.J., Giangola, G., Adelman, M.A. and Landis, R. (1994), "The cause of perioperative stroke after carotid endarterectomy." *Journal of vascular surgery: official publication, the Society for Vascular Surgery [and] International Society for Cardiovascular Surgery, North American Chapter*, vol. 19, 206.
- Shimizu, K., Matsuda, T., Sakurai, T., Fujita, A., Ohara, H., Okamura, S., Hashimoto, S., Mano, H., Kawai, C. and Kiri, M. (1986), "Visualization of moving fluid: quantitative analysis of blood flow velocity using MR imaging." *Radiology*, vol. 159, 195-199.
- Timoshenko, S. and Goodier, J. (1970), *Theory of Elasticity*, McGraw-Hill, New York.
- Tortoli, P., Bambi, G., Guidi, F. and Muchada, R. (2002), "Toward a better quantitative measurement of aortic flow." *Ultrasound Med Biol*, vol. 28, 249-257.